Palaeogeography, Palaeoclimatology, Palaeoecology
December 2022, Volume 607, Pages 111267 (12p.)
https://doi.org/10.1016/j.palaeo.2022.111267
https://archimer.ifremer.fr/doc/00798/90961/

Precession-driven changes in air-sea CO2 exchange by East Asian summer monsoon in the Western Tropical Pacific since MIS 6

Guo Jingteng [1, 2], Qiu Xiaohua [3], Algeo Thomas J. [4, 5], Li Tiegang [1, 2, *], Xiong Zhifang [1, 2], Zhao Debo [6], Dang Haowen [7], Qiao Peijun [7], Qin Bingbin [1], Jia Qi [1]

[1] Key Laboratory of Marine Geology and Metallogeny, First Institute of Oceanography, Ministry of Natural Resources, Qingdao 266061, China
[2] Laboratory for Marine Geology, Pilot National Laboratory for Marine Science and Technology (Qingdao), Qingdao 266237, China
[3] Shandong Institute of Geological Sciences, Jinan 250013, China
[4] Department of Geology, University of Cincinnati, Cincinnati, OH 45221-0013, USA
[5] State Key Laboratories of Biogeology and Environmental Geology, and Geological Processes and Mineral Resources, China University of Geosciences, Wuhan 430074, China
[6] Key laboratory of Marine Geology and Environment, Institute of Oceanology, Chinese Academy of Sciences, Qingdao 266071, China
[7] State Key Laboratory of Marine Geology, Tongji University, Shanghai 200092, China

* Corresponding author : Jingteng Li, email address : tgli@fio.org.cn

Abstract :

Surface waters of the modern Western Tropical Pacific (WTP) are in equilibrium with atmospheric CO2. However, air-sea exchange of CO2 in this region may have been modulated in the past by oceanic-atmospheric fluctuations in the tropical Pacific such as the East Asian monsoon and the El Niño-Southern Oscillation (ENSO) and extratropical mode waters such as Antarctic Intermediate Water. Thus, understanding controls on the sea-surface carbonate system in the WTP is important for forecasting future carbon-cycle changes in this region. Here, we reconstruct sea-surface pH and pCO2 since Marine Isotope Stage 6 (MIS 6; 155 ka) based on B/Ca ratios of the planktic foraminifer Globigerinoides ruber (white) in sediment Core MD06–3052 from the western Philippine Sea, and we then calculate the difference between oceanic and atmospheric pCO2 (ΔpCO2(sw-atm)) in order to evaluate the history of air-sea CO2 exchange. ΔpCO2(sw-atm) changes were strongly modulated by the ~20-kyr precession cycle. The results of cross-spectral analysis demonstrate a close connection between the East Asian summer monsoon (EASM) and air-sea CO2 exchange since MIS 6, demonstrating that precession-driven EASM can affect air-sea CO2 exchange through regulation of surface productivity and thermocline depth. In contrast, the East Asian winter monsoon (EAWM) and ENSO-like conditions are not major influences on air-sea CO2 exchange in the study area at precession-band frequencies. In addition, enhanced upwelling of Southern Ocean-sourced deepwater rich in dissolved inorganic carbon (DIC) affected the upper water column during transitions from cold to warm stages (i.e., deglaciations). In conclusion, these findings suggest that orbital precession influences can affect oceanic conditions not only through climate change and biological processes but also through sea-surface carbonate chemistry.

Highlights

► Reconstruction of sea-surface pH and pCO_2 in Western Tropical Pacific since MIS-6. ► EAWM and ENSO-like conditions do not affect $\Delta pCO_{2(sw\text{-}atm)}$ of WTP in precession band. ► Precession-driven EASM affects air-sea CO_2 exchange by regulating productivity & DOT. ► Surface carbonate system in WTP linked to upwelling of Southern Ocean deep waters. ► Upwelling strongest during cold-to-warm stage transitions (MIS 6/5, 5b/5a, 4/3, 2/1).

Keywords : planktic foraminifera, B/Ca, El Niño-Southern Oscillation, productivity, thermocline, precession

1. Introduction

Although details of the mechanisms are still emerging, fluctuations in the atmospheric partial pressure of carbon dioxide ($pCO_{2\text{-atm}}$) over the past 800,000 years can be attributed primarily to oceanic processes (Broecker, 1982; Sigman and Boyle, 2000; Lüthi et al., 2008; Sigman et al., 2010; Yu et al., 2020). Various paleoceanographic records from the Western Tropical Pacific (WTP), including productivity (Beaufort et al., 2001; Li et al., 2010; Bolliet et al., 2011; Diester-Haass et al., 2018), deep-water carbonate ion concentrations (Qin et al., 2017, 2018), redox-sensitive elements (Xiong et al., 2019; Xu et al., 2020), and terrigenous material inputs (Wan et al., 2017; Xu et al., 2020) have been investigated to improve our understanding of the relationships between $pCO_{2\text{-atm}}$ and oceanic conditions, confirming that processes in the WTP play a key role in $pCO_{2\text{-atm}}$ variation. Given direct contact of the surface ocean with the atmosphere, the carbonate chemistry of surface seawater is closely related to atmospheric pCO_2 levels. Hence, reconstructing sea-surface carbonate-system parameters is potentially a promising method for identifying the mechanisms and effects of CO_2 partitioning between atmosphere and ocean in the WTP.

The net air-sea CO_2 flux indicates that surface seawater of the modern WTP is in equilibrium with atmospheric pCO_2 (Takahashi et al., 2009), which might be taken as evidence that the surface seawater in this region has little influence on atmospheric CO_2 levels. However, tropical and extratropical influences may have played important roles in the air-sea CO_2 exchange of the WTP in the past (Beaufort et al., 2001; Feely et al., 2002; Anderson et al., 2009; Yuan et al., 2011; Xiong et al., 2022). Specifically, interannual-decadal variability in the El Niño-Southern Oscillation (ENSO) exerts a strong influence on air-sea

CO_2 exchange in this region. During El Niño (La Niña) conditions, this area is a weak CO_2 source (sink) to the atmospheric CO_2 reservoir due to thermocline shoaling (deepening) (Inoue and Sugimura, 1992; Feely et al., 2002). In addition, seasonal variations in the East Asian monsoon (EAM) not only affect air-sea CO_2 exchange but also regulate biological activity (Yuan et al., 2011). For example, East Asian summer monsoon (EASM)-induced upwelling brought nutrient- and DIC-rich deep waters to the surface, enhancing primary production and CO_2 release in coastal waters (Yin, 2002; Yuan et al., 2011). Southern Ocean-sourced watermasses such as Subantarctic Mode Water (SAMW) and Antarctic Intermediate Water (AAIW) can carry chemical signatures (e.g., nutrient- and CO_2-rich) from the upwelled deep watermass to low-latitude areas (Sarmiento et al., 2004), a process that promoted CO_2 release from the equatorial Pacific during the last deglaciation (Kubota et al., 2014, 2019). These processes regulate atmosphere CO_2 variation through the sea-surface carbonate system. However, previous studies have rarely used carbonate chemistry to link these influences with the record of secular $pCO_{2\text{-atm}}$ variation (Li et al., 2010; Xu et al., 2020), so the underlying controls on such variation remain incompletely understood.

Paleorecords related to the carbon cycle in the WTP, such as productivity and shell weight, exhibit considerable power at orbital periodicities, especially the ~20-kyr precession cycle (Beaufort et al., 2001; Fraser et al., 2014; Su et al., 2015; Qin et al., 2020). Although physical (e.g., upwelling) and biological (e.g., production) processes are known regulators of air-sea CO_2 exchange (Gottschalk et al., 2016; Gray et al., 2018), the detailed mechanisms and pathways by which orbital precession affects the carbon cycle in the WTP are not well-established. Late Quaternary strengthening of the EASM associated with precession

drove upwelling intensity, enhanced organic flux, and thermocline shoaling in the South China Sea (SCS) (Jian et al., 2001). In addition, ENSO activity exhibits pronounced precession-band variance in marine proxy records in the late Quaternary (Koutavas et al., 2002; Zhang et al., 2021b), with the potential to influence tropical Pacific surface productivity and thermoclinal depth (Su et al., 2015; Zhang et al., 2021b). Thus, orbital precession may regulate air-sea CO_2 exchange through links to monsoonal intensity, ENSO activity, surface productivity, and thermoclinal depth.

The main aim of the present study is to investigate the influence of the surface seawater carbonate system on air-sea CO_2 exchange in the WTP as well as the role of the tropical West Pacific in the global carbon cycle. Proxies for reconstructing past carbonate-system parameters have been developed in previous studies, including shell weight (Barker and Elderfield, 2002; Qin et al., 2017), boron isotopes ($\delta^{11}B$) (Hönisch and Hemming, 2005; Rae et al., 2018), and B/Ca (Yu et al., 2007; Dang et al., 2019; Guo et al., 2019; Osborne et al., 2020) of planktic foraminifera. The B/Ca proxy has been widely used owing to its relative speed, minimal sample consumption, and low cost, yielding records of sea-surface pH and pCO_2 (Yu et al., 2007; Foster, 2008; Tripati et al., 2009) and bottom-water [CO_3^{2-}] (Yu and Elderfield, 2007; Yu et al., 2020). In this paper, we analyzed B/Ca ratios of the planktic foraminifer *G. ruber* (white) in Core MD06-3052 from the western Philippine Sea (WPS). Combining Mg/Ca-paleothermometry and stable oxygen isotope measurements of *G. ruber* in Core MD06-3052 (Qiu et al., 2014a), we presented new sea-surface pH and pCO_2 records for the WTP since Marine Isotope Stage 6 (MIS 6). Together, these data allow us to (1) describe glacial-interglacial changes of the surface seawater carbonate system in the WTP; (2)

investigate the influence of various marine environmental factors on air-sea CO_2 exchange; and (3) identify possible controls on air-sea CO_2 exchange in the late Quaternary WTP.

2. Oceanographic setting

Core MD06-3052 is located in the WPS of the WTP, in the area affected by the bifurcation of the North Equatorial Current (NEC) (Figure 1a). The NEC separates into two branches near the eastern coast of the Philippine islands (Toole et al., 1990). The northward branch forms the main section of the Kuroshio Current (KC), whereas the southward branch produces the Mindanao Current (MC), which flows southward feeding the North Equatorial Counter Current (NECC) (Fig. 1a). The NEC bifurcation exhibits annual and seasonal changes in its latitudinal position owing to dynamic influences linked to ENSO and the East Asian monsoons (Kim et al., 2004; Hu et al., 2015). The NEC and its branches are the most important surface currents in the Philippine Sea. The intermediate circulation of the southern Philippine region is dominated by AAIW, which can be traced to about 12° N off Mindanao (Qu et al., 1999). Thus, AAIW may carry chemical signatures from upwelled deep waters of the Southern Ocean to the present study area (Sarmiento et al., 2004; Talley et al., 2011).

The difference between seawater pCO_2 ($pCO_{2\text{-sw}}$) and $pCO_{2\text{-atm}}$ across the air-sea interface ($\Delta pCO_{2(\text{sw-atm})}$) is the thermochemical driving potential for the net transfer of CO_2 between the atmosphere and the surface ocean, and it can be used to identify carbon sources and sinks (Takahashi et al., 2009). Geographic variation in mean annual $\Delta pCO_{2(\text{sw-atm})}$ for the modern tropical Pacific ranges from –50 ppmv to 100 ppmv, indicating that this region can act as a carbon sink or source of atmosphere CO_2 (Fig. S1; Takahashi et al., 2011). The major

carbon source area is observed in the Eastern Tropical Pacific (Fig. S1), which is an upwelling area that can bring deep waters with low pH and high $pCO_{2\text{-sw}}$ to the surface (Raven et al., 2005; Takahashi et al., 2009). The major carbon sink area is observed in the southwestern tropical Pacific (Fig. S1), which is a region of high biological production and export (Raven et al., 2005; Takahashi et al., 2009). In contrast, $\Delta pCO_{2(\text{sw-atm})}$ values in the WTP (including the WPS) are close to 0 ppmv, which indicates that air-sea CO_2 exchange in this region is in equilibrium.

3. Materials and methods

3.1 Materials

Core MD06-3052 was retrieved using a Calypso piston corer during the Chinese-French joint cruise Marco Polo 2 aboard the *R/V Marion Dufresne* in 2006. The core is located on the Bicol Shelf, offshore of Luzon Island, in the WPS at a water depth of 732 m (14°48.6042' N, 123°29.3983′ E) (Fig. 1). The dominant lithology is olive-gray to gray silty clay and silt. The age model of the study core is based on accelerator mass spectrometry (AMS) ^{14}C dates and correlation of the *G. ruber* $\delta^{18}O$ record with the standard $\delta^{18}O$ curve (Qiu et al., 2014a). Based thereon, this 19.48-m-long sediment core covers the last 155 kyr, from MIS 6 to the recent, accumulating at an average sedimentation rate of ~12.5 cm/kyr (Qiu et al., 2014a).

3.2 Foraminiferal B/Ca analysis

The studied core was subsampled at 8 cm intervals, yielding a total of 218 samples for foraminiferal B/Ca analysis. The samples were dried, disaggregated by soaking in water for

48 h, wet sieved (63-μm sieve), and dried again to collect the coarse fraction. Foraminiferal shells (approximately 40 tests per sample) of the planktic species *G. ruber* were picked from the 250-300 μm fraction, to minimize vital effects on shell geochemistry (Elderfield et al., 2002; Ni et al., 2007; Guo et al., 2015). Cleaning and B/Ca analysis of foraminiferal shells were conducted in the State Key Laboratory of Marine Geology, Tongji University, Shanghai. Before analysis, the foraminiferal tests were first gently cracked to open the individual chambers, then successively treated with methanol, hydrazine/ammonium citrate solution, and buffered H_2O_2 solution to remove clays, metal oxides and organic material, next leached with a 0.001 mol/L HNO_3 solution for removal of any adsorbed contaminants on the test fragments, and finally dissolved in 0.15 mol/L HNO_3 (Lea et al., 2000; Martin and Lea, 2002; Barker et al., 2003).

B/Ca ratios were analyzed on an inductively coupled plasma mass spectrometer (ICP-MS) following the method of Yu et al. (2005). All samples were analyzed at similar Ca concentrations (~100 ppm) to overcome potential matrix effects on B/Ca ratios. After every three samples, a standard (Check Std) was analyzed to monitor the accuracy of the results and to correct for drift and mass bias effects. A total of 125 analyses of the standard yielded a mean B/Ca value (110.641 μmol/mol) and relative standard deviation (0.635%) in conformity with its published composition (110.357 μmol/mol). The mean relative uncertainty of *G. ruber* B/Ca measurements is 2.4% (corresponding to 3.03 μmol/mol), as determined from replicate analyses of samples (n = 136) over the 14-month interval of analytical work. Al/Ca and Mn/Ca were also measured to monitor the efficiency of the removal steps for clays and Mn-oxyhydroxides. Neither Al/Ca nor Mn/Ca exhibits a correlation with B/Ca, indicating the

effectiveness of the cleaning method.

3.3 Estimation of seawater pH and pCO_2 from foraminiferal B/Ca

Based on the temperature (T) derived from *G. ruber* Mg/Ca in the Core MD06-3052 (Qiu et al., 2014a), the partition coefficient, K_D, between calcium carbonate and seawater was calculated as (Yu et al., 2007):

$$K_D(\times 1000) = (0.047 \pm 0.022)e^{(0.131 \pm 0.017)T} \quad (1)$$

Combined with the B/Ca ratio of the planktic foraminifer *G. ruber* from Core MD06-3052, the $[B(OH)_4^-/HCO_3^-]$ of surface seawater in the WTP was then obtained as (Hemming and Hanson, 1992; Yu et al., 2007):

$$[B(OH)_4^-/HCO_3^-]_{seawater} = [B/Ca]_{CaCO_3} / K_D \quad (2)$$

Following the method given in Hönisch and Hemming (2005), two models were employed to calculate surface seawater salinity (SSS) and total alkalinity (ALK) in the WTP. In the first model, $\delta^{18}O_{sw\text{-}iv}$ was first obtained using $\delta^{18}O$ and Mg/Ca data measured in *G. ruber* from Core MD06-3052 (Qiu et al., 2014a) by removing temperature and global ice volume effects following the method of Bemis et al. (1998) and Waelbroeck et al. (2002), and the local SSS was then calculated by the following equation (Xiong et al., 2022):

$$SSS = [(14.244 \pm 0.961) + \delta^{18}O_{sw\text{-}iv}] / (0.424 \pm 0.029) \quad (3)$$

In the second model, SSS was estimated using the relative sea level (RSL) (Waelbroeck et al., 2002; Hönisch and Hemming, 2005). In both models, ALK was estimated as (Xiong et al., 2022):

$$ALK = (70.22 \pm 3.01) \times SSS - (154.42 \pm 103.24) \quad (4)$$

Based on the above processes, we reconstructed sea-surface pH and pCO_2 in the tropical West Pacific using two methods. In the first method (Tripati et al., 2009), 'practical alkalinity' is used as an approximation for ALK in seawater (Eq. 5; Zeebe and Wolf-Gladrow, 2001):

$$[ALK] = [HCO_3^-] + 2[CO_3^{2-}] + [B(OH)_4^-] + [OH^-] - [H^+] \quad (5)$$

Equations (6)-(9) are then substituted into Equation (5):

$$[CO_3^{2-}] = [HCO_3^-] \times K_2/[H^+] \quad (6)$$

$$[B(OH)_4^-] = [B_{tot}] \times K_B/([H^+] + K_B) \quad (7)$$

$$[OH^-] = K_w/[H^+] \quad (8)$$

$$[HCO_3^-] = K_B \times B_{tot} \times ([H^+] + K_B) \times ([B(OH)_4^-]/[HCO_3^-]) \quad (9)$$

We obtained a third-order polynomial equation with a single unknown ($[H^+]$) by algebraic manipulation of the resultant equation. Finally, the surface seawater pH in the WTP since MIS 6 was determined by solving this polynomial equation for the unknown ($[H^+]$). Based on ALK and pH in addition to temperature, salinity, and pressure (depth), $pCO_{2\text{-sw}}$ can be calculated using CO_2sys.xls (Pelletier et al., 2007).

The second method for reconstructing sea-surface pH and pCO_2 is based on an iterative method (Yu et al., 2007). First, $B(OH)_4^-$ is calculated from Equation (7) using an assumed pH value. Second, given ALK, temperature, salinity, and pressure (depth), along with estimated pH, it is possible to calculate $pCO_{2\text{-sw}}$ and HCO_3^- using CO_2sys.xls (Pelletier et al., 2007), from which $B(OH)_4^-/ HCO_3^-$ is then determined. Third, B/Ca ratios are calculated from Equation (2) and compared with the measured B/Ca ratios. Finally, the sequence of steps above are iterated until calculated and measured B/Ca ratios converge, yielding the most robust estimates of sea-surface pH and pCO_2.

The calculations for estimating sea-surface pH and pCO_2 in the tropical West Pacific made use of carbonate dissociation constants K_1 and K_2 from Mehrbach et al. (1973) as refitted by Lueker et al. (2000), K_B and K_w from DOE (1994), K_{SO4} from Dickson (1990), $[B]_{tot}$ from Lee et al. (2010), and total pH scale. Four pH, $pCO_{2\text{-sw}}$ and $\Delta pCO_{2(\text{sw-atm})}$ records were generated based on the two models for salinity estimation and the two pH-pCO_2 calculation methods. For records of pH, $pCO_{2\text{-sw}}$ and $\Delta pCO_{2(\text{sw-atm})}$, the uncertainty produced by the four results calculated from the two models for SSS and two calculation methods is negligible (Fig. S2). Hence, we present only the records calculated by using the $\delta^{18}O$-derived SSS and the iterative calculation method to illustrate the variations of the surface seawater carbonate system in the WTP since MIS 6 (Fig. 2).

The total uncertainty of the reconstructed pH and $pCO_{2\text{-sw}}$ values is based on the propagated 2σ uncertainties of B/Ca, SST, SSS, and ALK. This calculation made use of initial uncertainties of ±3.03 μmol/mol for B/Ca, ±0.07 mmol/mol for Mg/Ca, and ±0.06‰ for $\delta^{18}O$, which yielded uncertainties of ±0.2 °C for SST, ±0.5 psu for SSS, and ±34 μmol/kg for ALK. These values are small compared to the errors of ±1 °C in SST, ±1 psu in SSS, and ±100 μmol/kg applied in some recent studies (Hönisch et al., 2019; Xiong et al., 2022), so we chose the larger (i.e., published) uncertainties for our error propagation. The final errors associated with pH and $pCO_{2\text{-sw}}$ are ±0.073 units in pH and ±65.5 ppmv in $pCO_{2\text{-sw}}$ on average, propagated from the individual uncertainties of B/Ca (±3.03 μmol/mol, corresponding to ±0.011 units in pH and ±9.7 ppmv in $pCO_{2\text{-sw}}$ on average), SST (±1 °C, corresponding to ±0.069 units in pH and ±63.6 ppmv in $pCO_{2\text{-sw}}$ on average), SSS (±1 psu, corresponding to ±0.006 units in pH and ±11.8 ppmv in $pCO_{2\text{-sw}}$ on average), and ALK (±100

μmol/kg, corresponding to ±0.020 units in pH and ±3.6 ppmv in $pCO_{2\text{-sw}}$ on average).

3.4 Caveats

Although the benthic foraminiferal B/Ca proxy has been well calibrated and widely applied in paleoceanographic studies (e.g., Yu and Elderfield, 2007; Yu et al., 2014), controls on the planktic foraminiferal B/Ca proxy have yet to be fully identified. There are two forms of dissolved boron in seawater: $B(OH)_4^-$ and $B(OH)_3$, the proportions of which are highly pH-dependent (Hershey et al., 1986). Because $B(OH)_4^-$ is the main species incorporated into carbonates, seawater paleo-pH can be estimated using the B/Ca ratios of planktic foraminifera given an accurate constraint on K_D in Equation (2) (Hemming and Hanson, 1992; Yu et al., 2007). Since K_D is thought to be temperature-dependent (Yu et al., 2007), questions have arisen regarding use of the planktic B/Ca proxy. Various studies have reported both positive and negative correlations between K_D and temperature (Yu et al., 2007; Foster, 2008; Tripati et al., 2009). Foster (2008) found that seawater $[CO_3^{2-}]$ also can affect K_D. In addition, DIC (Allen and Hönisch, 2012; Haynes et al., 2017), light intensity (Babila et al., 2014), $[PO_4^{3-}]$ (Henehan et al., 2015), growth and calcification rates (Ni et al., 2007; Salmon et al., 2016), and salinity (Allen et al., 2011; Henehan et al., 2015) have been reported as influencing the incorporation of boron into foraminiferal calcite. However, culture experiments have inferred that temperature has little influence on K_D (Allen et al., 2011), and that shell growth rate does not appear to determine B/Ca ratios (Haynes et al., 2017).

Although interpretation of the planktic B/Ca proxy may be controversial due to its possible dependence on vital effects and/or various seawater physicochemical properties (Ni

et al., 2007; Salmon et al., 2016; Haynes et al., 2017), this proxy is known to respond to variation in sea-surface pH and, thus, permits reconstruction of paleo-$pCO_{2\text{-sw}}$ (Yu et al., 2007; Foster, 2008; Yu et al., 2013; Guo et al., 2019). Considering the uncertainties surrounding the application of the planktic B/Ca proxy, it is crucial to assess the reliability of B/Ca-based pH estimates. This can be achieved using foraminiferal $\delta^{11}B$ (Yu et al., 2010, 2013), which is a well-established and non-controversial proxy for seawater pH (Hemming and Hanson, 1992; Hönisch and Hemming, 2005; Foster and Rae, 2016). To evaluate the robustness of planktic B/Ca for reconstruction of seawater pH in the study area, we compared sea-surface pH and pCO_2 as reconstructed from $\delta^{11}B$ in the nearby Core MD06-3054 (Xiong et al., 2022) with our B/Ca-based pH and $pCO_{2\text{-sw}}$ estimates (Figs. 1 and S3). This comparison shows that nearly indistinguishable pH and $pCO_{2\text{-sw}}$ estimates are obtained from $\delta^{11}B$ and B/Ca, yielding similar trends and absolute values, which proves that planktic foraminiferal B/Ca ratios can serve as a reliable proxy for sea-surface pH in the study area.

3.5 Cross-spectral analysis and filters

Cross-spectral analysis of $\Delta pCO_{2(\text{sw-atm})}$ versus proxies for the EAM and ENSO-like conditions was undertaken with the ARAND software package (Howell et al., 2006). The bandwidth was 0.0222. All data series were linearly interpolated at 1 kyr intervals and detrended prior to analysis. Because the study interval in Core MD06-3052 spans only the last 155 kyr, it was not possible to examine coherence between proxy records and the 100-kyr orbital eccentricity cycle at the 95% confidence level. Thus, our analysis of orbital forcing of oceanographic conditions in the WPS focuses exclusively on the ~20-kyr precession cycle.

Gaussian band-pass filters were applied to the $\Delta pCO_{2(sw\text{-}atm)}$ and published proxy records using the Acycle software (Li et al., 2019) to extract oscillations associated with precessional periodicities. The center frequency of the filters was 0.043 kyr^{-1} and the bandwidth was 0.003.

4. Results

B/Ca ratios in *G. ruber* from Core MD06-3052 since MIS 6 range between 83 and 143 μmol/mol, with significant differences between glacial and interglacial stages (Fig. 2b). Specifically, B/Ca ratios are high in MIS 5e and MIS 1, and low in MIS 6 and MIS 5d-2. In addition, B/Ca ratios show a decrease from MIS 5 to MIS 2 as well as a prominent increase during the MIS 6/5 and MIS 2/1 deglaciations (Fig. 2b). Sea-surface pH in the WTP since MIS 6 also exhibits significant variations between glacial and interglacial stages, showing an inverse correlation with B/Ca and pCO_2 (Fig. 2). pH ranges from 7.97 to 8.31, being low in MIS 5e and MIS 1, and high in MIS 6 and MIS 5d-2 (Fig. 2c). Contrary to B/Ca, the pH values in the WTP show a long-term rise from MIS 5 to MIS 2 as well as significant decreases during the MIS 6/5 and MIS 2/1 deglaciations (Fig. 2c).

The $pCO_{2\text{-}sw}$ record derived from B/Ca shows a similar trend with that of $pCO_{2\text{-}atm}$ (Bereiter et al., 2015) (Fig. 2d). Furthermore, within uncertainty, $pCO_{2\text{-}sw}$ is in equilibrium with, or higher than, coeval $pCO_{2\text{-}atm}$ (Fig. 2d). To examine this relationship in more details, we calculated the difference between $pCO_{2\text{-}sw}$ and $pCO_{2\text{-}atm}$ (i.e., $\Delta pCO_{2(sw\text{-}atm)}$) (Fig. 2e). The $\Delta pCO_{2(sw\text{-}atm)}$ is roughly equal to 0 ppmv in the late Holocene (i.e., 3-0 ka), indicating equilibrium between $pCO_{2\text{-}sw}$ and $pCO_{2\text{-}atm}$, which conforms to proxy records of net air-sea

CO_2 flux in the WTP for this interval (Takahashi et al., 2009) and demonstrates the reliability of the reconstructed sea-surface pH and pCO_2 values derived from Core MD06-3052. This air-sea CO_2 equilibrium has prevailed since MIS 6 except for relatively brief intervals during MIS 6, MIS 5e, MIS 4/3, and MIS 2/1 when the WTP has served as a transient, modest CO_2 source (Fig. 2e).

5. Discussion

5.1 Mechanisms for air-sea CO_2 exchange in the WPS since MIS 6

Our reconstructed $\Delta pCO_{2(sw\text{-}atm)}$ record reveals that the WTP has been in air-sea CO_2 equilibrium, or has served as a modest CO_2 source, since MIS 6 (Fig. 2e). During the transient intervals in which CO_2 was sourced from the WTP, oceanic processes may have contributed to the disequilibrium in CO_2 exchange between ocean and atmosphere. Air-sea CO_2 exchange in the modern WTP is known to be influenced by the EAM and ENSO (Feely et al., 2002; Zhai et al., 2009; Yuan et al., 2011), the past behavior of which can be reconstructed from various types of proxy records. For example, a composite stalagmite $\delta^{18}O$ record from Chinese caves characterizes changes in EASM wind intensity over the past 640 kyr (Cheng et al., 2016), and grain-size variation (GT32, >32 μm particle content) on the Chinese Loess Plateau records variation in the East Asian winter monsoon (EAWM) over the past 880 kyr (Hao et al., 2012). In addition, the experiments of Clement et al. (1999) with the Zebiak-Cane ENSO model incorporating Milankovitch solar forcing yielded the NINO 3 index for ENSO-like conditions. To investigate the effects of EAM and ENSO-like conditions on air-sea CO_2 exchange in the study area since MIS 6, we compared the reconstructed

$\Delta pCO_{2(sw\text{-}atm)}$ record of Core MD06-3052 with stalagmite $\delta^{18}O$ (Cheng et al., 2016), GT32 (Hao et al., 2012), and the NINO 3 index (Clement et al., 1999) (Fig. 3).

5.1.1 ENSO-like conditions

In the modern, ENSO controls air-sea CO_2 exchange in the WTP through lateral advection of surface waters from the Eastern Tropical Pacific and regulation of the depth of thermocline (DOT) within the WTP (Inoue and Sugimura, 1992; Feely et al., 2002; Ishii et al., 2014; Chiodi and Harrison, 2015; Chen et al., 2016). The modern Eastern Tropical Pacific, which is characterized by high $pCO_{2\text{-}sw}$, is a major source of CO_2 to the atmosphere, and the area of the source region extends westward during La Niña periods and retreats eastward during El Niño periods (Inoue and Sugimura, 1992; Takahashi et al., 2009; Ishii et al., 2014). During westward expansions, high $pCO_{2\text{-}sw}$ surface waters extend only to the easternmost WTP and, thus, do not influence $\Delta pCO_{2(sw\text{-}atm)}$ in the WPS (Xiong et al., 2022). For this reason, ENSO in the modern ocean exerts a large impact on air-sea CO_2 exchange in the study area mainly through its influence on DOT (Inoue and Sugimura, 1992; Feely et al., 2002; Chiodi and Harrison, 2015; Chen et al., 2016). Specifically, El Niño periods are characterized by thermoclinal shallowing, which brings nutrient- and CO_2-rich subsurface waters to the surface, charging the latter with CO_2 and promoting increases in productivity and $\Delta pCO_{2(sw\text{-}atm)}$. In contrast, La Niña periods are characterized by thermoclinal deepening, which limits migration of CO_2 and nutrients between the thermocline and surface watermass, resulting in lower $pCO_{2\text{-}sw}$, productivity and $\Delta pCO_{2(sw\text{-}atm)}$ in surface waters of the study area (Inoue and Sugimura, 1992; Turk et al., 2001; Feely et al., 2002; Xiong et al., 2022).

Variation in the $\Delta pCO_{2(sw\text{-}atm)}$ record of this study matches that of the NINO 3 index since MIS 6 (Clement et al., 1999), i.e., higher $\Delta pCO_{2(sw\text{-}atm)}$ corresponds to La Niña-like conditions (Fig. 3a, f). Furthermore, the spectrum of $\Delta pCO_{2(sw\text{-}atm)}$ is dominated by a strong precessional (~20 kyr) signal (Fig. 4, red line), and cross-spectral analysis of $\Delta pCO_{2(sw\text{-}atm)}$ (Fig. 3f) and the NINO 3 index (Clement et al., 1999) (Fig. 3a) reveals that the former proxy is anti-phased with the simulated ENSO record in the precession-band frequency range at the 95% confidence level (Fig. 4a), meaning that higher $\Delta pCO_{2(sw\text{-}atm)}$ in the study area is correlated with La Niña-like conditions since MIS 6. However, this relationship is the opposite of that between ENSO and $\Delta pCO_{2(sw\text{-}atm)}$ prevailing in the study area today, in which higher (lower) $\Delta pCO_{2(sw\text{-}atm)}$ is related to El Niño (La Niña) periods. Thus, we infer that ENSO-like conditions are unlikely to have been the main cause for $\Delta pCO_{2(sw\text{-}atm)}$ variation at precession-band frequencies in the study area since MIS 6.

5.1.2 East Asian Monsoon

In the modern, the EAWM causes a negative wind stress curl that enhances Ekman downwelling, causing the WTP to be a moderate sink for atmospheric CO_2 (Tozuka et al., 2002; Xiong et al., 2022). However, records from Core MD06-3052 indicate that the WTP was in air-sea CO_2 equilibrium or served as a modest CO_2 source during MIS 6, MIS 5e, MIS 4/3, and MIS 2/1 (Fig. 2e). In addition, unlike the covariation between $\Delta pCO_{2(sw\text{-}atm)}$ and ENSO-like conditions, the cross-spectral analysis between $\Delta pCO_{2(sw\text{-}atm)}$ (Fig. 3f) and GT32 in the Luochuan loess section (Hao et al., 2012) (Fig. 3b) displays insignificant coherence in the precession band (Fig. 4b). Hence, we infer that the EAWM has had little effect on air-sea

CO_2 exchange at precession-band frequencies in the study area since MIS 6.

The climatic interpretation of Chinese cave $\delta^{18}O$ records remains a subject of intense debate, with various studies proposing influence by rainfall amount, recycling of terrestrial precipitation, moisture-source temperature, and moisture source region and transport pathway (e.g., Maher and Thompson, 2012; Parker et al., 2021; Tan, 2014). However, a nascent consensus has emerged based on data-model approaches that interpret Chinese cave $\delta^{18}O$ as a record of summer monsoon intensity driven by upstream depletion of moisture, with high (low) $\delta^{18}O$ values reflecting weak (strong) EASM intensity (e.g., Cheng et al., 2016, 2019, 2021; Liu et al., 2014; Liu et al., 2020; Wen et al., 2016, He et al., 2021; Zhang et al., 2019, 2021a). In the modern, the EASM is characterized by a positive wind stress curl that results in Ekman upwelling in the study area (Tozuka et al., 2002; Xiong et al., 2022). Ekman upwelling is accompanied by thermocline shoaling that brings nutrient- and CO_2-rich subsurface waters to the surface layer, enhancing $pCO_{2\text{-sw}}$ and primary productivity (Tozuka et al., 2002; Raven et al., 2005; Takahashi et al., 2009). Our records show that $\Delta pCO_{2(\text{sw-atm})}$ in the study area has been in good agreement with EASM intensity since MIS 6, i.e., higher $\Delta pCO_{2(\text{sw-atm})}$ corresponds to a stronger EASM (Fig. 3c, f). This relationship implies that physical CO_2 degassing has been more important than biological carbon sequestration in the study area since MIS 6. In addition, cross-spectral analysis between $\Delta pCO_{2(\text{sw-atm})}$ (Fig. 3f) and stalagmite $\delta^{18}O$ (Cheng et al., 2016) (Fig. 3c) reveals anti-phased variation in the precession-band frequency range at the 95% confidence level (Fig. 4c), confirming the relationship of higher $\Delta pCO_{2(\text{sw-atm})}$ to stronger EASM. Thus, based on a comparison of paleorecords and the results of cross-spectral analysis, we infer that variations of $\Delta pCO_{2(\text{sw-atm})}$

in the study area since MIS 6 were closely related to EASM intensity in the precession band, with higher $\Delta pCO_{2(sw\text{-}atm)}$ linked to a stronger EASM.

In order to explore the close connection between air-sea CO_2 exchange in the study area and EASM intensity at precession-band frequencies since MIS 6, we investigated secular variation in DOT and primary productivity. The difference in Mg/Ca-based temperatures between surface-dwelling species (e.g., *G. ruber*) and thermocline-dwelling species (e.g., *Neogloboquadrina dutertrei* and *Pulleniatina obliquiloculata*) has been widely used to track changes in upper water column structure (Steinke et al., 2010; Hollstein et al., 2018; Jian et al., 2020; Zhang et al., 2021b). Specifically, a larger (smaller) temperature difference (ΔT) between sea-surface temperature (SST) and thermocline water temperature (TWT) denotes a larger (smaller) vertical temperature gradient and, thus, a shallower (deeper) thermocline (Hollstein et al., 2018; Jian et al., 2020). Spectral analysis of the ΔT record of Core MD06-3052 previously revealed peaks in the orbital precession band (Qiu, 2013) (Fig. S4a). We applied Gaussian band-pass filters to the stalagmite $\delta^{18}O$ (Cheng et al., 2016) (Fig. 3c) and Core MD06-3052 ΔT records (Qiu, 2013) (Fig. 3d), and the results show that DOT generally varied in phase with EASM intensity (Fig. 3c, d), confirming the relationship between these parameters at precession-band frequencies in the study area since MIS 6.

The orbital precession cycle has been found in records of late Pleistocene primary productivity in the study area (Fraser et al., 2014) (Fig. S4b), which is in accordance with other records from the WTP (Beaufort et al., 2001; Su et al., 2015). The precessional filter for primary productivity (Fraser et al., 2014) is strongly correlated with stalagmite $\delta^{18}O$ (Cheng et al., 2016) (Fig. 3c, e), indicating a close connection between productivity and EASM

intensity. Therefore, we infer that primary productivity variation in the study area was mainly controlled by EASM intensity rather than ENSO-like conditions at precession-band frequencies since MIS 6, with higher (lower) primary productivity corresponding to a stronger (weaker) EASM.

Variation in EASM intensity on orbital timescales is thought to be modulated primarily by precession-paced insolation (Kutzbach et al., 2008; Wang et al., 2008). Specifically, an increase of precession-dominated Northern Hemisphere summer insolation (NHSI) results in a stronger EASM (Wang et al., 2008). Analogous to the modern, EASM strengthening is accompanied by thermoclinal shoaling and Ekman upwelling that brings nutrient- and CO_2-rich subsurface waters to the surface layer (Tozuka et al., 2002; Raven et al., 2005; Takahashi et al., 2009), leading to higher primary productivity and $pCO_{2\text{-sw}}$ in the surface watermass (Fig. 3c-e). Finally, physical CO_2 degassing exceeds biological carbon sequestration in the study area, generating higher $\Delta pCO_{2(\text{sw-atm})}$ at precession-band frequencies since MIS 6 (Fig. 3f). As a result, the study area has served as a modest CO_2 source, especially during transient intervals of MIS 6, MIS 5e, and MIS 2/1 (Fig. 3f). By contrast, a decrease of precession-driven NHSI caused weaker EASM, which was accompanied by thermoclinal deepening and reduced primary productivity and $pCO_{2\text{-sw}}$ in surface waters of the study area, generating lower $\Delta pCO_{2(\text{sw-atm})}$ at precession-band frequencies since MIS 6 (Fig. 3c-f). Finally, lower $\Delta pCO_{2(\text{sw-atm})}$ led to air-sea CO_2 equilibrium in the study area within uncertainty (Fig. 3f).

5.2 Control of air-sea CO_2 exchange during cold-to-warm stage transitions (deglaciations)

The temporal agreement between marine records of the Eastern Tropical Pacific and ice-core records of Antarctica suggests that deglacial $\delta^{13}C$ minimum signals generated at high latitudes can be laterally advected to the tropical Pacific by enhanced SAMW/AAIW flow and atmospheric CO_2 (Spero and Lea, 2002). Planktic foraminiferal $\delta^{13}C$ minima are also observed at the transitions from cold to warm stages (i.e., MIS 6/5, MIS 4/3 and MIS 2/1) in the study area (Qiu et al., 2014b) (Fig. 5c), coincident with extreme values of sea-surface pH and $pCO_{2\text{-sw}}$ in the study core (Fig. 2c, d). Since the formation of North Pacific Intermediate Water was weak and the influence of AAIW was stronger during the last deglaciation in the study area (Kubota et al., 2015; Yang et al., 2017), we infer that the extreme values of sea-surface pH, $pCO_{2\text{-sw}}$, and $\delta^{13}C$ in the WTP record increased upwelling and/or ventilation of the Southern Ocean during the glacial-interglacial transitions, and that AAIW carried the chemical signature from the Southern Ocean to our study area (see Section 2; Qu et al., 1999; Sarmiento et al., 2004; Talley et al., 2011).

In order to further investigate whether DIC was transmitted to our study area by enhanced AAIW flow, we explored the relationship of our reconstructed $\Delta pCO_{2(\text{sw-atm})}$ profile to both the planktic foraminiferal $\delta^{13}C$ record of study Core MD06-3052 (Qiu et al., 2014b) and the opal flux records of reference Cores TN057-13PC, TN057-14PC, and ODP 1094 in the Southern Ocean (Anderson et al., 2009; Jaccard et al., 2013) (Fig. 5). These results show that peak values of opal flux correspond to low values of $\delta^{13}C$ and high values of $\Delta pCO_{2(\text{sw-atm})}$ during glacial-interglacial transitions (i.e., MIS 6/5, MIS 5b/5a, MIS 4/3, and MIS 2/1; cyan bars of Fig. 5). In addition, $\delta^{13}C$ minima in the thermocline-dwelling species *N. dutertrei* from study Core MD06-3052 during the transitions has also been reported in a

previous study (Qiu, 2013). This observation implies that, as a consequence of increased ventilation of the Southern Ocean, DIC-rich AAIW diffused into the thermocline of the WTP, affecting its upper water column and air-sea CO_2 exchange (Kubota et al., 2014; Martínez-Botí et al., 2015). Therefore, we infer that changes in air-sea CO_2 exchange in the WTP during cold-to-warm stage transitions (i.e., MIS 6/5, MIS 5b/5a, MIS 4/3, and MIS 2/1) were related to the increased ventilation of deep waters in the Southern Ocean.

5.3 Significance of precessional forcing for paleoclimate

Changes in upwelling rates associated with precession-driven monsoonal intensity have been documented in the Indo-Pacific region on orbital timescales (Jian et al., 2001; Lückge et al., 2009; Wang et al., 2018). In addition, precessional forcing of ENSO-like conditions and tropical climate has been proposed on the basis of model experiments and instrumental records (Clement et al., 1999; Lu et al., 2019; Zhang et al., 2021). Furthermore, variations in productivity associated with monsoonal intensity and ENSO-like conditions are thus linked to precessional forcing, as confirmed by previous studies in the Indo-Pacific region (Beaufort et al., 2001; Lückge et al., 2009; Su et al., 2015). Hence, the Earth's orbital precession can effect climate change by modulating both physical (e.g., monsoon intensity, upwelling rates) and biological (e.g., productivity rates) processes. In the present study, our planktic foraminiferal B/Ca record from Core MD06-3052 demonstrates that $\Delta pCO_{2(sw\text{-}atm)}$ was also controlled by precessional forcing, which means that, in addition to physical and biological processes, precession can also effect climate change through chemical processes (cf. Zhao et al., 2021). In conclusion, precession can exert a large impact on climate change including

air-sea CO_2 exchange by regulating physical (e.g., monsoon intensity, upwelling rates), biological (e.g., productivity rates), and chemical (e.g., surface carbonate chemistry) processes.

6. Conclusions

On the basis of B/Ca measurements for the planktic foraminifer *G. ruber* from Core MD06-3052 in the WTP, we calculated sea-surface pH and $pCO_{2\text{-sw}}$, and investigated the relationship between marine environmental factors and air-sea CO_2 exchange in the study area since MIS 6. The major conclusions are summarized as follows:

(1) Sea-surface pH and $pCO_{2\text{-sw}}$ in the Western Tropical Pacific (WTP) since MIS 6 exhibit significant variations between glacial and interglacial stages, although $\Delta pCO_{2(\text{sw-atm})}$ records suggest that the WTP has been in air-sea CO_2 equilibrium or has served as a modest CO_2 sink since MIS 6 (~155 ka).

(2) In the precession-band frequency range, EAWM and ENSO-like conditions have not been the main control on air-sea CO_2 exchange in the study area since MIS 6. However, air-sea CO_2 exchange has been modulated by precession-driven EASM intensity. Precession-dominated stronger (weaker) EASM was associated with thermoclinal shallowing (deepening), increases (reductions) in primary productivity, and higher (lower) $\Delta pCO_{2(\text{sw-atm})}$.

(3) DIC-rich AAIW has diffused into the thermocline of the WTP during intervals of increased ventilation of the Southern Ocean, affecting sea-surface pH and $pCO_{2\text{-sw}}$ in the study area during cold-to-warm stage (glacial to interglacial) transitions, including MIS 6/5, MIS 5b/5a, MIS 4/3, and MIS 2/1.

Acknowledgments

We are grateful to Xufeng Zheng and Xingxing Wang for their support on data calculation and error analysis. We thank editors Mary Elliot and Jie Huang and two anonymous reviewers for their constructive comments, which helped to improve our manuscript. This study was supported by the National Natural Science Foundation of China (NSFC, Grant no. 41830539), the Marine S&T Fund of Shandong Province for Pilot National Laboratory for Marine Science and Technology (Qingdao) (Grant no. 2022QNLM050203), Evaluation and Effect of Paleoclimatic Evolution (Grant no. GASI-04-QYQH-04), NSFC (Grant nos. 91858106, 42006075, and 41976080), the Taishan Scholars Project Funding (Grant no. ts20190963), and the Basic Scientific Fund for National Public Research Institutes of China (Grant nos. 2019S04, 2017Y07, GY0222Q06, and 2019Q09).

References

Allen, K.A., Hönisch, B., 2012. The planktic foraminiferal B/Ca proxy for seawater carbonate chemistry: A critical evaluation. Earth and Planetary Science Letters 345, 203-211.

Allen, K.A., Hönisch, B., Eggins, S.M., Yu, J., Spero, H.J., Elderfield, H., 2011. Controls on boron incorporation in cultured tests of the planktic foraminifer *Orbulina universa*. Earth and Planetary Science Letters 309, 291-301.

Anderson, R., Ali, S., Bradtmiller, L., Nielsen, S., Fleisher, M., Anderson, B., Burckle, L., 2009. Wind-driven upwelling in the Southern Ocean and the deglacial rise in

atmospheric CO_2. Science 323, 1443-1448.

Babila, T.L., Rosenthal, Y., Conte, M.H., 2014. Evaluation of the biogeochemical controls on B/Ca of *Globigerinoides ruber* white from the Oceanic Flux Program, Bermuda. Earth and Planetary Science Letters 404, 67-76.

Barker, S., Elderfield, H., 2002. Foraminiferal calcification response to glacial-interglacial changes in atmospheric CO_2. Science 297, 833-836.

Barker, S., Greaves, M., Elderfield, H., 2003. A study of cleaning procedures used for foraminiferal Mg/Ca paleothermometry. Geochemistry, Geophysics, Geosystems 4, 8407. doi:10.1029/2003GC000559.

Beaufort, L., de Garidel-Thoron, T., Mix, A.C., Pisias, N.G., 2001. ENSO-like forcing on oceanic primary production during the late Pleistocene. Science 293, 2440-2444.

Bemis, B.E., Spero, H.J., Bijma, J., Lea, D.W., 1998. Reevaluation of the oxygen isotopic composition of planktonic foraminifera: Experimental results and revised paleotemperature equations. Paleoceanography 13, 150-160.

Bereiter, B., Eggleston, S., Schmitt, J., Nehrbass-Ahles, C., Stocker, T.F., Fischer, H., Kipfstuhl, S., Chappellaz, J., 2015. Revision of the EPICA Dome C CO_2 record from 800 to 600 kyr before present. Geophysical Research Letters 42, 542-549.

Bolliet, T., Holbourn, A., Kuhnt, W., Laj, C., Kissel, C., Beaufort, L., Kienast, M., Andersen, N., Garbe-Schönberg, D., 2011. Mindanao Dome variability over the last 160 kyr: Episodic glacial cooling of the West Pacific Warm Pool. Paleoceanography 26, PA1208. doi:10.1029/2010PA001966.

Broecker, W.S., 1982. Glacial to interglacial changes in ocean chemistry. Progress in

Oceanography 11, 151-197.

Cannariato, K., Ravelo, A., 1997. Pliocene-Pleistocene evolution of eastern tropical Pacific surface water circulation and thermocline depth. Paleoceanography 12, 805-820.

Chaisson, W., Ravelo, A., 2000. Pliocene development of the east-west hydrographic gradient in the equatorial Pacific. Paleoceanography 15, 497-505.

Chen, M., Li, T., Shen, X., Wu, B., 2016. Relative roles of dynamic and thermodynamic processes in causing evolution asymmetry between El Niño and La Niña. Journal of Climate 29, 2201-2220.

Cheng, H., Edwards, R.L., Sinha, A., Spötl, C., Yi, L., Chen, S., Kelly, M., Kathayat, G., Wang, X., Li, X., Kong, X., Wang, Y., Ning, Y., Zhang, H., 2016. The Asian monsoon over the past 640,000 years and ice age terminations. Nature 534, 640-646.

Cheng, H., Zhang, H., Cai, Y., Shi, Z., Yi, L., Deng, C., Hao, Q., Peng, Y., Sinha, A., Li, H., Zhao, J., Tian, Y., Baker, J., Perez-Mejías, C., 2021. Orbital-scale Asian summer monsoon variations: Paradox and exploration. Science China Earth Sciences 64, 529-544.

Cheng, H., Zhang, H., Zhao, J., Li, H., Ning, Y., Kathayat, G., 2019. Chinese stalagmite paleoclimate researches: A review and perspective. Science China Earth Sciences 62, 1489-1513.

Chiodi, A.M., Harrison, D.E., 2015. Global seasonal precipitation anomalies robustly associated with El Niño and La Niña events—An OLR perspective. Journal of Climate 28, 6133-6159.

Clement, A.C., Seager, R., Cane, M.A., 1999. Orbital controls on the El Niño/Southern

Oscillation and the tropical climate. Paleoceanography 14, 441-456.

Dang, H., Wang, T., Qiao, P., Bassinot, F., Jian, Z., 2019. The B/Ca and Cd/Ca of a subsurface-dwelling foraminifera *Pulleniatina obliquiloculata* in the tropical Indo-Pacific Ocean: implications for the subsurface carbonate chemistry estimation. Acta Oceanologica Sinica 38, 138-150.

Dickson, A.G., 1990. Standard potential of the reaction: AgCl(s) + ½ H_2(g) = Ag(s) + HCl(aq), and and the standard acidity constant of the ion HSO_4^- in synthetic sea water from 273.15 to 318.15 K. The Journal of Chemical Thermodynamics 22, 113-127.

Diester-Haass, L., Billups, K., Lear, C., 2018. Productivity changes across the mid-Pleistocene climate transition. Earth-Science Reviews 179, 372-391.

D.O.E., 1994. Handbook of Methods for the Analysis of the Various Parameters of the Carbon Dioxide System in Sea Water; version 2. A. G. Dickson & C. Goyet (eds.), ORNL/CDIAC-74, U.S. Department of Energy.

Elderfield, H., Vautravers, M., Cooper, M., 2002. The relationship between shell size and Mg/Ca, Sr/Ca, $\delta^{18}O$, and $\delta^{13}C$ of species of planktonic foraminifera. Geochemistry, Geophysics, Geosystems 3, 1-13.

Feely, R.A., Boutin, J., Cosca, C.E., Dandonneau, Y., Etcheto, J., Inoue, H.Y., Ishii, M., Le Quéré, C., Mackey, D.J., McPhaden, M., 2002. Seasonal and interannual variability of CO_2 in the equatorial Pacific. Deep Sea Research Part II: Topical Studies in Oceanography 49, 2443-2469.

Foster, G.L., 2008. Seawater pH, pCO_2 and [CO_3^{2-}] variations in the Caribbean Sea over the last 130 kyr: A boron isotope and B/Ca study of planktic forminifera. Earth and

Planetary Science Letters 271, 254-266.

Foster, G.L., Rae, J.W., 2016. Reconstructing ocean pH with boron isotopes in foraminifera. Annual Review of Earth and Planetary Sciences 44, 207-237.

Fraser, N., Kuhnt, W., Holbourn, A., Bolliet, T., Andersen, N., Blanz, T., Beaufort, L., 2014. Precipitation variability within the West Pacific Warm Pool over the past 120 ka: Evidence from the Davao Gulf, southern Philippines. Paleoceanography 29, 1094-1110.

Gottschalk, J., Skinner, L.C., Lippold, J., Vogel, H., Frank, N., Jaccard, S.L., Waelbroeck, C., 2016. Biological and physical controls in the Southern Ocean on past millennial-scale atmospheric CO_2 changes. Nature Communications 7. doi: 10.1038/ncomms11539.

Gray, W.R., Rae, J.W.B., Wills, R.C.J., Shevenell, A.E., Taylor, B., Burke, A., Foster, G.L., Lear, C.H., 2018. Deglacial upwelling, productivity and CO_2 outgassing in the North Pacific Ocean. Nature Geoscience 11, 340-344.

Guo, J., Li, T., Yu, X., Xiong, Z., Chang, F., 2015. A preliminary evaluation on B/Ca of planktic foraminifera as a proxy for seawater pH: Vital effects and dissolution. Marine Geology & Quaternary Geology 35, 109-118 (in Chinese with English abstract).

Guo, J., Li, T., Xiong, Z., Qiu, X., Chang, F., 2019. Revisiting the dependence of thermocline-dwelling foraminiferal B/Ca on temperature and [CO_3^{2-}], and its application in reconstruction of the subsurface carbonate system in the tropical western Pacific since 24 ka. Acta Oceanologica Sinica 38, 71-86.

Hao, Q., Wang, L., Oldfield, F., Peng, S., Qin, L., Song, Y., Xu, B., Qiao, Y., Bloemendal, J., Guo, Z., 2012. Delayed build-up of Arctic ice sheets during 400,000-year minima in insolation variability. Nature 490, 393-396.

Haynes, L.L., Hönisch, B., Dyez, K.A., Holland, K., Rosenthal, Y., Fish, C.R., Subhas, A.V., Rae, J.W., 2017. Calibration of the B/Ca proxy in the planktic foraminifer *Orbulina universa* to Paleocene seawater conditions. Paleoceanography 32. doi:10.1002/2016PA003069.

He, C., Liu, Z., Otto-Bliesner, B., Brady, E., Zhu, C., Tomas, R., Clark, P., Zhu, J., Jahn, A., Gu, S., Zhang, J., Nusbaumer, J., Noone, D., Cheng, H., Wang, Y., Yan, M., Bao, Y., 2021. Hydroclimate footprint of pan-asian monsoon water isotope during the last deglaciation. Science Advances 7, eabe2611. doi: 10.1126/sciadv.abe2611.

Hemming, N., Hanson, G., 1992. Boron isotopic composition and concentration in modern marine carbonates. Geochimica et Cosmochimica Acta 56, 537-543.

Henehan, M.J., Foster, G.L., Rae, J.W., Prentice, K.C., Erez, J., Bostock, H.C., Marshall, B.J., Wilson, P.A., 2015. Evaluating the utility of B/Ca ratios in planktic foraminifera as a proxy for the carbonate system: A case study of *Globigerinoides ruber*. Geochemistry, Geophysics, Geosystems 16, 1052-1069.

Hershey, J.P., Fernandez, M., Milne, P.J., Millero, F.J., 1986. The ionization of boric acid in NaCl, Na-Ca-Cl and Na-Mg-Cl solutions at 25°C. Geochimica et Cosmochimica Acta 50, 143-148.

Hollstein, M., Mohtadi, M., Rosenthal, Y., Prange, M., Oppo, D.W., Martínez Méndez, G., Tachikawa, K., Moffa Sanchez, P., Steinke, S., Hebbeln, D., 2018. Variations in Western Pacific Warm Pool surface and thermocline conditions over the past 110,000 years: Forcing mechanisms and implications for the glacial Walker circulation. Quaternary Science Reviews 201, 429-445.

Hönisch, B., Eggins, S.M., Haynes, L.L., Allen, K.A., Holland, K.D., Lorbacher, K., 2019. Boron proxies in paleoceanography and paleoclimatology. John Wiley and Sons, Ltd. Hoboken, New Jersey, 227 pp.

Hönisch, B., Hemming, N.G., 2005. Surface ocean pH response to variations in pCO_2 through two full glacial cycles. Earth and Planetary Science Letters 236, 305-314.

Howell, P., Pisias, N., Ballance, J., Baughman, J., Ochs, L., 2006. ARAND time-series analysis software. Brown University, Providence, Rhode Island.

Hu, D., Wu, L., Cai, W., Gupta, A.S., Ganachaud, A., Qiu, B., Gordon, A.L., Lin, X., Chen, Z., Hu, S., 2015. Pacific western boundary currents and their roles in climate. Nature 522, 299-308.

Inoue, H.Y., Sugimura, Y., 1992. Variations and distributions of CO_2 in and over the equatorial Pacific during the period from the 1986/88 El Niño event to the 1988/89 La Niña event*. Tellus B 44, 1-22.

Ishii, M., Feely, R., Rodgers, K., Park, G.-H., Wanninkhof, R., Sasano, D., Sugimoto, H., Cosca, C., Nakaoka, S.-I., Telszewski, M., 2014. Air–sea CO_2 flux in the Pacific Ocean for the period 1990–2009. Biogeosciences 11, 709-734.

Jaccard, S., Hayes, C.T., Martínez-García, A., Hodell, D., Anderson, R.F., Sigman, D., Haug, G., 2013. Two modes of change in Southern Ocean productivity over the past million years. Science 339, 1419-1423.

Jian, Z., Huang, B., Kuhnt, W., Lin, H.-L., 2001. Late Quaternary upwelling intensity and East Asian monsoon forcing in the South China Sea. Quaternary Research 55, 363-370.

Jian, Z., Wang, Y., Dang, H., Lea, D.W., Liu, Z., Jin, H., Yin, Y., 2020. Half-precessional

cycle of thermocline temperature in the western equatorial Pacific and its bihemispheric dynamics. Proceedings of the National Academy of Sciences (U.S.A.) 117, 7044-7051.

Kim, Y.Y., Qu, T., Jensen, T., Miyama, T., Mitsudera, H., Kang, H.W., Ishida, A., 2004. Seasonal and interannual variations of the North Equatorial Current bifurcation in a high-resolution OGCM. Journal of Geophysical Research Oceans 109, C3040. doi:3010.1029/2003JC002013.

Koutavas, A., Lynch-Stieglitz, J., Marchitto, T.M., Sachs, J.P., 2002. El Niño-like pattern in ice age tropical Pacific sea surface temperature. Science 297, 226-230.

Kubota, K., Yokoyama, Y., Ishikawa, T., Obrochta, S., Suzuki, A., 2014. Larger CO_2 source at the equatorial Pacific during the last deglaciation. Scientific Reports 4, 5261. doi:10.1038/srep05261.

Kubota, Y., Kimoto, K., Itaki, T., Yokoyama, Y., Miyairi, Y., Matsuzaki, H., 2015. Bottom water variability in the subtropical northwestern Pacific from 26 kyr BP to present based on Mg/Ca and stable carbon and oxygen isotopes of benthic foraminifera. Climate of the Past 11, 803-824.

Kubota, K., Yokoyama, Y., Ishikawa, T., Sagawa, T., Ikehara, M., Yamazaki, T., 2019. Equatorial Pacific seawater pCO_2 variability since the last glacial period. Scientific Reports 9, 13814. doi: 10.1038/s41598-019-49739-0.

Kutzbach, J.E., Liu, X., Liu, Z., Chen, G., 2008. Simulation of the evolutionary response of global summer monsoons to orbital forcing over the past 280,000 years. Climate Dynamics 30, 567-579.

Lea, D.W., Pak, D.K., Spero, H.J., 2000. Climate impact of late Quaternary equatorial Pacific

sea surface temperature variations. Science 289, 1719-1724.

Lee, K., Kim, T.-W., Byrne, R.H., Millero, F.J., Feely, R.A., Liu, Y.-M., 2010. The universal ratio of boron to chlorinity for the North Pacific and North Atlantic oceans. Geochimica et Cosmochimica Acta 74, 1801-1811.

Li, M., Hinnov, L., Kump, L., 2019. Acycle: Time-series analysis software for paleoclimate research and education. Computers & Geosciences 127, 12-22.

Li, T., Zhao, J., Sun, R., Chang, F., Sun, H., 2010. The variation of upper ocean structure and paleoproductivity in the Kuroshio source region during the last 200 kyr. Marine Micropaleontology 75, 50-61.

Liu, X., Liu, J., Chen, S., Chen, J., Zhang, X., Yan, J., Chen, F., 2020. New insights on Chinese cave $\delta^{18}O$ records and their paleoclimatic significance. Earth-Science Reviews 207, 103216. doi: 10.1016/j.earscirev.2020.103216.

Liu, Z., Wen, X., Brady, E. C., Otto-Bliesner, B., Yu, G., Lu, H., Cheng, H., Wang, Y., Zheng, W., Ding, Y., Edwards, R.L., Cheng, J., Liu, W., Yang, H., 2014. Chinese cave records and the East Asia Summer Monsoon. Quaternary Science Reviews 83, 115-128.

Lu, Z., Liu, Z., Chen, G., Guan, J., 2019. Prominent precession band variance in ENSO intensity over the last 300,000 years. Geophysical Research Letters 46, 9786-9795.

Lückge, A., Mohtadi, M., Rühlemann, C., Scheeder, G., Vink, A., Reinhardt, L., Wiedicke, M., 2009. Monsoon versus ocean circulation controls on paleoenvironmental conditions off southern Sumatra during the past 300,000 years. Paleoceanography 24, PA1208. doi:10.1029/2008PA001627.

Lueker, T.J., Dickson, A.G., Keeling, C.D., 2000. Ocean pCO_2 calculated from dissolved

inorganic carbon, alkalinity, and equations for K_1 and K_2: validation based on laboratory measurements of CO_2 in gas and seawater at equilibrium. Marine Chemistry 70, 105-119.

Lüthi, D., Le Floch, M., Bereiter, B., Blunier, T., Barnola, J.-M., Siegenthaler, U., Raynaud, D., Jouzel, J., Fischer, H., Kawamura, K., 2008. High-resolution carbon dioxide concentration record 650,000–800,000 years before present. Nature 453, 379-382.

Maher B.A., Thompson R., 2012. Oxygen isotopes from Chinese caves: records not of monsoon rainfall but of circulation regime. Journal of Quaternary Science 27, 615-624.

Martin, P.A., Lea, D.W., 2002. A simple evaluation of cleaning procedures on fossil benthic foraminiferal Mg/Ca. Geochemistry, Geophysics, Geosystems 3, 1-8.

Martínez-Botí, M., Marino, G., Foster, G., Ziveri, P., Henehan, M., Rae, J., Mortyn, P., Vance, D., 2015. Boron isotope evidence for oceanic carbon dioxide leakage during the last deglaciation. Nature 518, 219-222.

Mehrbach, C., Culberson, C.H., Hawley, J.E., Pytkowic, R.M., 1973. Measurement of the apparent dissociation constants of carbonic acid in seawater at atmospheric pressure. Limnology and Oceanography 18, 897-907.

Ni, Y., Foster, G.L., Bailey, T., Elliott, T., Schmidt, D.N., Pearson, P., Haley, B., Coath, C., 2007. A core top assessment of proxies for the ocean carbonate system in surface-dwelling foraminifers. Paleoceanography 22, PA3212. doi:3210.1029/2006PA001337.

Osborne, E.B., Umling, N.E., Bizimis, M., Buckley, W., Sadekov, A., Tappa, E., Marshall, B., Sautter, L.R., Thunell, R.C., 2020. A sediment trap evaluation of B/Ca as a carbonate system proxy in asymbiotic and nondinoflagellate hosting planktonic foraminifera.

Paleoceanography and Paleoclimatology 35. doi/10.1029/2019PA003682.

Parker, S. E., Harrison, S. P., Comas-Bru, L., Kaushal, N., Legrande, A. N., Werner, M., 2021. A data–model approach to interpreting speleothem oxygen isotope records from monsoon regions. Climate of the Past 17, 1119-1138.

Pelletier, G., Lewis, E., Wallace, D., 2007. CO2SYS. XLS: A calculator for the CO_2 system in seawater for Microsoft Excel/VBA. Washington State Department of Ecology/Brookhaven National Laboratory, Olympia, WA/Upton, NY, USA.

Qin, B., Li, T., Xiong, Z., Algeo, T.J., Chang, F., 2017. Deepwater carbonate ion concentrations in the WTP since 250 ka: Evidence for oceanic carbon storage and global climate influence. Paleoceanography 32, 351-370.

Qin, B., Li, T., Xiong, Z., Algeo, T.J., Jia, Q., 2018. Deep-water carbonate ion concentrations in the WTP since the mid-Pleistocene: A major perturbation during the mid-Brunhes. Journal of Geophysical Research: Oceans 123, 6876-6892.

Qin, B., Li, T., Xiong, Z., Algeo, T.J., Jia, Q., 2020. Calcification of planktonic foraminifer *Pulleniatina obliquiloculata* controlled by seawater temperature rather than ocean acidification. Global and Planetary Change 193, 103256. doi: 10.1016/j.gloplacha.2020.103256.

Qiu, X., 2013. The paleoceanographic records during the past 150 kyr B.P. in the northern part of western Pacific Warm Pool. Doctoral thesis, Institute of Oceanology, Chinese Academy of Sciences, Qingdao.

Qiu, X., Li, T., Chang, F., Nan, Q., Xiong, Z., Sun, H., 2014a. Sea surface temperature and salinity reconstruction based on stable isotopes and Mg/Ca of planktonic foraminifera in

the western Pacific Warm Pool during the last 155 ka. Chinese Journal of Oceanology and Limnology 32, 187-200.

Qiu, X., Li, T., Nan, Q., Gong, H., 2014b. Carbon isotope minimum events in the northern margin of western Pacific Warm Pool since during the past 150 ka. Marine Sciences, 116-121 (in Chinese with English abstract).

Qu, T., Mitsudera, H., Yamagata, T., 1999. A climatology of the circulation and water mass distribution near the Philippine coast. Journal of Physical Oceanography 29, 1488-1505.

Rae, J.W.B., Burke, A., Robinson, L.F., Adkins, J.F., Chen, T., Cole, C., Greenop, R., Li, T., Littley, E.F.M., Nita, D.C., Stewart, J.A., Taylor, B.J., 2018. CO_2 storage and release in the deep Southern Ocean on millennial to centennial timescales. Nature 562, 569-573.

Ravelo, A., Andreasen, D., 1999. Using planktonic foraminifera as monitors of the tropical surface ocean. *In*: Abrantes, F., Mix, A.C. (eds.), Reconstructing Ocean History: A Window into the Future, Springer, pp. 217-243.

Raven, J., Caldeira, K., Elderfield, H., Hoegh-Guldberg, O., Liss, P., Riebesell, U., Shepherd, J., Turley, C., Watson, A., 2005. Ocean acidification due to increasing atmospheric carbon dioxide. The Royal Society, London, UK, 68 pp. ISBN 0-85403-617-2.

Salmon, K.H., Anand, P., Sexton, P.F., Conte, M., 2016. Calcification and growth processes in planktonic foraminifera complicate the use of B/Ca and U/Ca as carbonate chemistry proxies. Earth and Planetary Science Letters 449, 372-381.

Sarmiento, J.L., Gruber, N., Brzezinski, M., Dunne, J., 2004. High-latitude controls of thermocline nutrients and low latitude biological productivity. Nature 427, 56-60.

Schlitzer, R., 2021. Ocean Data View, v.5.5.1-64 bit (Windows), https://odv.awi.de.

Sigman, D.M., Boyle, E.A., 2000. Glacial/interglacial variations in atmospheric carbon dioxide. Nature 407, 859-869.

Sigman, D.M., Hain, M.P., Haug, G.H., 2010. The polar ocean and glacial cycles in atmospheric CO_2 concentration. Nature 466, 47-55.

Spero, H.J., Lea, D.W., 2002. The cause of carbon isotope minimum events on glacial terminations. Science 296, 522-525.

Steinke, S., Mohtadi, M., Groeneveld, J., Lin, L.-C., Löwemark, L., Chen, M.-T., Rendle-Bühring, R., 2010. Reconstructing the southern South China Sea upper water column structure since the Last Glacial Maximum: Implications for the East Asian winter monsoon development. Paleoceanography 25, PA2219. doi:10.1029/2009PA001850.

Su, X., Liu, C., Beaufort, L., Barbarin, N., Jian, Z., 2015. Differences in Late Quaternary primary productivity between the WTP and the South China Sea: Evidence from coccoliths. Deep Sea Research Part II: Topical Studies in Oceanography 122, 131-141.

Takahashi, T., Sutherland, S.C., Wanninkhof, R., Sweeney, C., Feely, R.A., Chipman, D.W., Hales, B., Friederich, G., Chavez, F., Sabine, C., 2009. Climatological mean and decadal change in surface ocean pCO_2, and net sea–air CO_2 flux over the global oceans. Deep Sea Research Part II: Topical Studies in Oceanography 56, 554-577.

Takahashi, T., Sutherland, S.C., Kozyr, A., 2011. Global Ocean Surface Water Partial Pressure of CO_2 Database: Measurements Performed During 1957–2010 (Version 2010). ORNL/CDIAC-159, NDP-088(V2010). Carbon Dioxide Information Analysis Center, Oak Ridge National Laboratory, U.S. Department of Energy, Oak Ridge, Tennessee, doi:

10.3334/CDIAC/otg.ndp088(V2010).

Talley, L.D., Pickard, G.L., Emery, W.J., Swift, J.H., 2011. Chapter 10 - Pacific Ocean, in: Talley, L.D., Pickard, G.L., Emery, W.J., Swift, J.H. (eds.), Descriptive Physical Oceanography (Sixth Edition). Academic Press, Boston, pp. 303-362.

Tan, M., 2014. Circulation effect: response of precipitation $\delta^{18}O$ to the ENSO cycle in monsoon regions of China. Climate Dynamics 42, 1067–1077.

Toole, J.M., Millard, R.C., Wang, Z., Pu, S., 1990. Observations of the Pacific North Equatorial Current bifurcation at the Philippine coast. Journal of Physical Oceanography 20, 307-318.

Tozuka, T., Kagimoto, T., Masumoto, Y., Yamagata, T., 2002. Simulated multiscale variations in the WTP: The Mindanao Dome revisited. Journal of Physical Oceanography 32, 1338-1359.

Tripati, A.K., Roberts, C.D., Eagle, R.A., 2009. Coupling of CO_2 and ice sheet stability over major climate transitions of the last 20 million years. Science 326, 1394-1397.

Turk, D., Lewis, M.R., Harrison, G.W., Kawano, T., Asanuma, I., 2001. Geographical distribution of new production in the western/central equatorial Pacific during El Niño and non-El Niño conditions. Journal of Geophysical Research: Oceans 106, 4501-4515.

Waelbroeck, C., Labeyrie, L., Michel, E., Duplessy, J.C., McManus, J.F., Lambeck, K., Balbon, E., Labracherie, M., 2002. Sea-level and deep water temperature changes derived from benthic foraminifera isotopic records. Quaternary Science Reviews 21, 295-305.

Wan, S., Clift, P.D., Zhao, D., Hovius, N., Munhoven, G., France-Lanord, C., Wang, Y.,

Xiong, Z., Huang, J., Yu, Z., Zhang, J., Ma, W., Zhang, G., Li, A., Li, T., 2017. Enhanced silicate weathering of tropical shelf sediments exposed during glacial lowstands: A sink for atmospheric CO_2. Geochimica et Cosmochimica Acta 200, 123-144.

Wang, X., Jian, Z., Lückge, A., Wang, Y., Dang, H., Mohtadi, M., 2018. Precession-paced thermocline water temperature changes in response to upwelling conditions off southern Sumatra over the past 300,000 years. Quaternary Science Reviews 192, 123-134.

Wang, Y., Cheng, H., Edwards, R.L., Kong, X., Shao, X., Chen, S., Wu, J., Jiang, X., Wang, X., An, Z., 2008. Millennial- and orbital-scale changes in the East Asian monsoon over the past 224,000 years. Nature 451, 1090-1093.

Wen, X., Liu, Z., Wang, S., Cheng, J., Zhu, J., 2016. Correlation and anti-correlation of the East Asian summer and winter monsoons during the last 21,000 years. Nature Communications 7, 1-7.

Xiong, Z., Li, T., Algeo, T.J., Nan, Q., Zhai, B., Lu, B., 2012. Paleoproductivity and paleoredox conditions during late Pleistocene accumulation of laminated diatom mats in the tropical West Pacific. Chemical Geology 334, 77-91.

Xiong, Z., Li, T., Hönisch, B., Algeo, T.J., Bradtmiller, L., Cane, M., Laj, C., Wang, F., Lu, Z., Qin, B., Chang, F., Gong, X., 2022. Monsoon- and ENSO-driven surface-water pCO_2 variation in the tropical West Pacific since the Last Glacial Maximum. Quaternary Science Reviews 289, 107621. doi: 10.1016/j.quascirev.2022.107621.

Xu, Z., Wan, S., Colin, C., Li, T., Clift, P.D., Chang, F., Sun, R., Yu, Z., Lim, D., 2020. Enhanced terrigenous organic matter input and productivity on the western margin of the

Western Pacific Warm Pool during the Quaternary sea-level lowstands: Forcing mechanisms and implications for the global carbon cycle. Quaternary Science Reviews 232, 106211. doi: 10.1016/j.quascirev.2020.106211.

Yang, Y., Xiang, R., Liu, J., Fu, S., Zhou, L., Du, S., Lü, H., 2017. Changes in intermediate water conditions in the northern South China Sea using *Globorotalia inflata* over the last 20 ka. Journal of Quaternary Science 32, 1037-1048.

Yin, K., 2002. Monsoonal influence on seasonal variations in nutrients and phytoplankton biomass in coastal waters of Hong Kong in the vicinity of the Pearl River estuary. Marine Ecology Progress Series 245, 111-122.

Yu, J., Anderson, R.F., Rohling, E.J., 2014. Deep ocean carbonate chemistry and glacial-interglacial atmospheric CO_2 changes. Oceanography 27, 16-25.

Yu, J., Elderfield, H., 2007. Benthic foraminiferal B/Ca ratios reflect deep water carbonate saturation state. Earth and Planetary Science Letters 258, 73-86.

Yu, J., Day, J., Greaves, M., Elderfield, H., 2005. Determination of multiple element/calcium ratios in foraminiferal calcite by quadrupole ICP-MS. Geochemistry, Geophysics, Geosystems 6, Q08P01. doi:10.1029/2005GC000964.

Yu, J., Elderfield, H., Hönisch, B., 2007. B/Ca in planktonic foraminifera as a proxy for surface seawater pH. Paleoceanography 22, PA2202. doi:10.1029/2006PA001347.

Yu, J., Foster, G.L., Elderfield, H., Broecker, W.S., Clark, E., 2010. An evaluation of benthic foraminiferal B/Ca and $\delta^{11}B$ for deep ocean carbonate ion and pH reconstructions. Earth and Planetary Science Letters 293, 114-120.

Yu, J., Thornalley, D.J., Rae, J.W., McCave, N.I., 2013. Calibration and application of B/Ca,

Cd/Ca, and $\delta^{11}B$ in *Neogloboquadrina pachyderma* (sinistral) to constrain CO_2 uptake in the subpolar North Atlantic during the last deglaciation. Paleoceanography 28, 237-252.

Yu, J., Menviel, L., Jin, Z.D., Anderson, R.F., Jian, Z., Piotrowski, A.M., Ma, X., Rohling, E.J., Zhang, F., Marino, G., McManus, J.F., 2020. Last glacial atmospheric CO_2 decline due to widespread Pacific deep-water expansion. Nature Geoscience 13, 628-633.

Yuan, X.-C., Yin, K., Cai, W.-J., Ho, A., Xu, J., Harrison, P.J., 2011. Influence of seasonal monsoons on net community production and CO_2 in subtropical Hong Kong coastal waters. Biogeosciences 8, 289-300.

Zeebe, R.E., Wolf-Gladrow, D.A., 2001. CO_2 in Seawater: Equilibrium, Kinetics, Isotopes. Elsevier, Amesterdam, 346 pp.

Zhai, W., Dai, M., Cai, W.-J., 2009. Coupling of surface pCO_2 and dissolved oxygen in the northern South China Sea: impacts of contrasting coastal processes. Biogeosciences 6, 2589-2598.

Zhang, H., Ait Brahim, Y., Li, N., Zhao, J., Kathayat, G., Tian, Y., Baker, J., Wang, J., Zhang, F., Ning, Y., Edwards, R.L., Cheng, H., 2019. The Asian summer monsoon: Teleconnections and forcing mechanisms—A review from Chinese speleothem $\delta^{18}O$ records. Quaternary 2, 26. doi:10.3390/quat2030026.

Zhang, H., Zhang, X., Cai, Y., Sinha, A., Spötl, C., Baker, J., Kathayat, G., Liu, Z., Tian, Y., Lu, J., Wang, Z., Zhao, J., Jia, X., Du, W., Ning, Y., An, Z., Edwards, R.L., Cheng, H., 2021a. A data–model comparison pinpoints Holocene spatiotemporal pattern of East Asian summer monsoon. Quaternary Science Reviews 261, 106911. doi: 10.1016/j.quascirev.2021.106911.

Zhang, S., Yu, Z., Gong, X., Wang, Y., Chang, F., Lohmman, G., Qi, Y., Li, T., 2021b. Precession cycles of the El Niño/Southern oscillation-like system controlled by Pacific upper-ocean stratification. Communications Earth & Environment 2, 239. doi: 10.1038/s43247-021-00305-5.

Zhao, D., Wan, S., Lu, Z., Zhai, L., Feng, X., Shi, X., Li, A., 2021. Delayed collapse of the North Pacific Intermediate Water after the glacial termination. Geophysical Research Letters 48, e2021GL092911, doi: 10.1029/2021GL092911.

Figure captions

Fig. 1. (a) Locations of cores MD06-3052 (this study), MD06-3054 (Xiong et al., 2022), and MD06-3075 (Fraser et al., 2014) and regional circulation in the WTP. NEC—North Equatorial Current, NECC—North Equatorial Counter Current, KC—Kuroshio Current, MC—Mindanao Current, ME—Mindanao Eddy, HE—Halmahera Eddy, and AAIW—Antarctic Intermediate Water. (b) Locations of reference cores TN057-13PC (same location as ODP 1094) and TN057-14PC in the Southern Ocean (Anderson et al., 2009; Jaccard et al., 2013). Maps were generated using Ocean Data View (Schlitzer, 2021).

Fig. 2. Reconstructed carbonate chemistry in Core MD06-3052 from the WTP. (a) $\delta^{18}O$ (Qiu et al., 2014a) and (b) B/Ca ratios in *G. ruber* (this study). (c) pH estimated from *G. ruber* B/Ca (this study). (d) $pCO_{2\text{-atm}}$ (Bereiter et al., 2015) and $pCO_{2\text{-sw}}$ (this study). (e)

$\Delta pCO_{2(sw\text{-}atm)}$ in Core MD06-3052 (this study). The blue dashed line in (e) corresponds to $\Delta pCO_{2(sw\text{-}atm)}$ = 0 ppmv. Colored shading for individual records indicates error ranges. The numbers at top in figures 2 to 5 denote marine isotope stages.

Fig. 3. Comparisons of $\Delta pCO_{2(sw\text{-}atm)}$ with EAM, ENSO-like conditions, temperature difference (ΔT), and primary productivity in the WTP. (a) 500-year average NINO 3 index in Zebiak-Cane model forced with Milankovitch solar forcing (Clement et al., 1999). (b) GT32 (>32 μm particle size) in the Luochuan loess section (Hao et al., 2012). (c) Composite stalagmite $\delta^{18}O$ record (Cheng et al., 2016). (d) Temperature difference (ΔT) between sea-surface temperature (SST) and thermocline water temperature (TWT) (Qiu, 2013). (e) Productivity estimated from the relative abundance of *Florisphaera profunda* in Core MD06-3075 (Fraser et al., 2014). (f) $\Delta pCO_{2(sw\text{-}atm)}$ in Core MD06-3052 (this study). The green line in (f) represents $\Delta pCO_{2(sw\text{-}atm)}$ = 0 ppmv, and the green dashed lines in (f) bracket the average error (±65.5 ppmv) associated with $\Delta pCO_{2(sw\text{-}atm)}$ estimates. The superimposed black lines denote the Gaussian band-pass filters (center frequency = 0.043 kyr^{-1}; bandwidth = 0.003).

Fig. 4. Cross-spectral analysis between $\Delta pCO_{2(sw\text{-}atm)}$ and proxies of EAM and ENSO-like conditions using the ARAND software package (Howell et al., 2006). (a) 500-year average NINO 3 index in Zebiak-Cane model forced with Milankovitch solar forcing (Clement et al., 1999) and $\Delta pCO_{2(sw\text{-}atm)}$. (b) GT32 (>32 μm particle content) in the Luochuan loess section (Hao et al., 2012) and $\Delta pCO_{2(sw\text{-}atm)}$. (c) Composite stalagmite $\delta^{18}O$ record (Cheng et al., 2016)

and $\Delta pCO_{2(sw\text{-}atm)}$. The bandwidth is 0.0222. All data have been linearly interpolated at 1 kyr and detrended prior to analysis. Dashed gray lines denote the 80% and 95% confidence levels. Cyan-shaded vertical bars indicate periods with significant coherence at the 95% confidence level. Vertical black bars are error bars.

Fig. 5. Coupling between ventilation of deep water in the Southern Ocean and air-sea CO_2 exchange in the study area. (a) $\delta^{18}O$ in *G. ruber* from Core MD06-3052 (Qiu et al., 2014a). (b) $\Delta pCO_{2(sw\text{-}atm)}$ in Core MD06-3052 (this study) (c) $\delta^{13}C$ in *G. ruber* from Core MD06-3052 (Qiu et al., 2014b). (d) Opal flux from Cores TN057-13PC, TN057-14PC, and ODP 1094 in the Southern Ocean (Anderson et al., 2009; Jaccard et al., 2013). Cyan bars indicate periods of increased ventilation in the Southern Ocean.

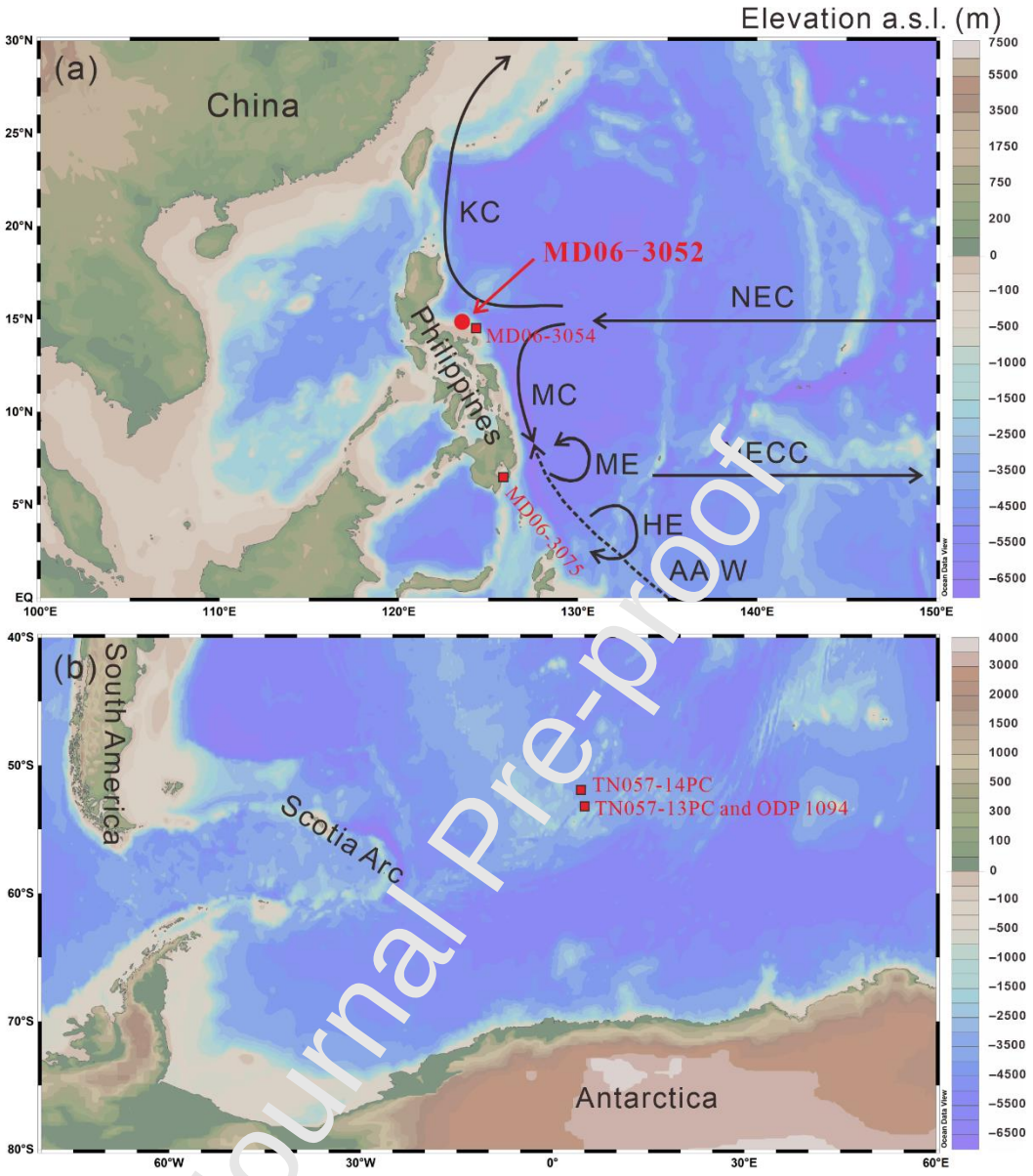

Fig. 1

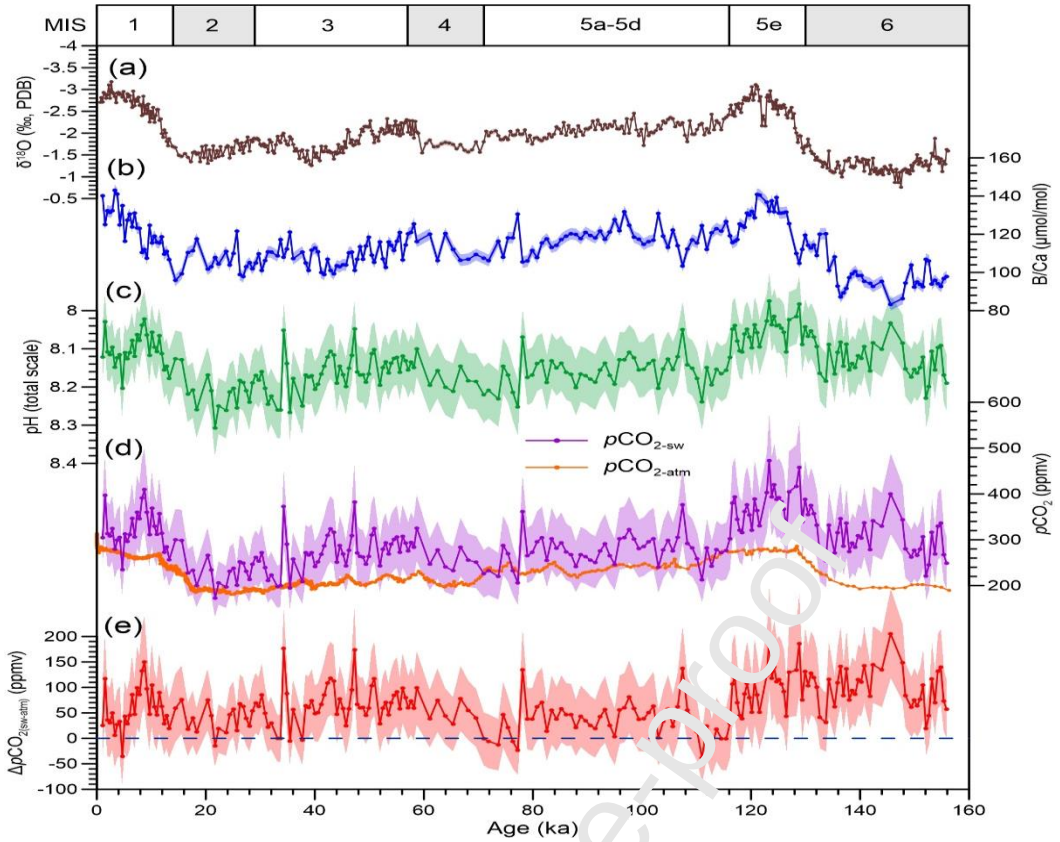

Fig. 2

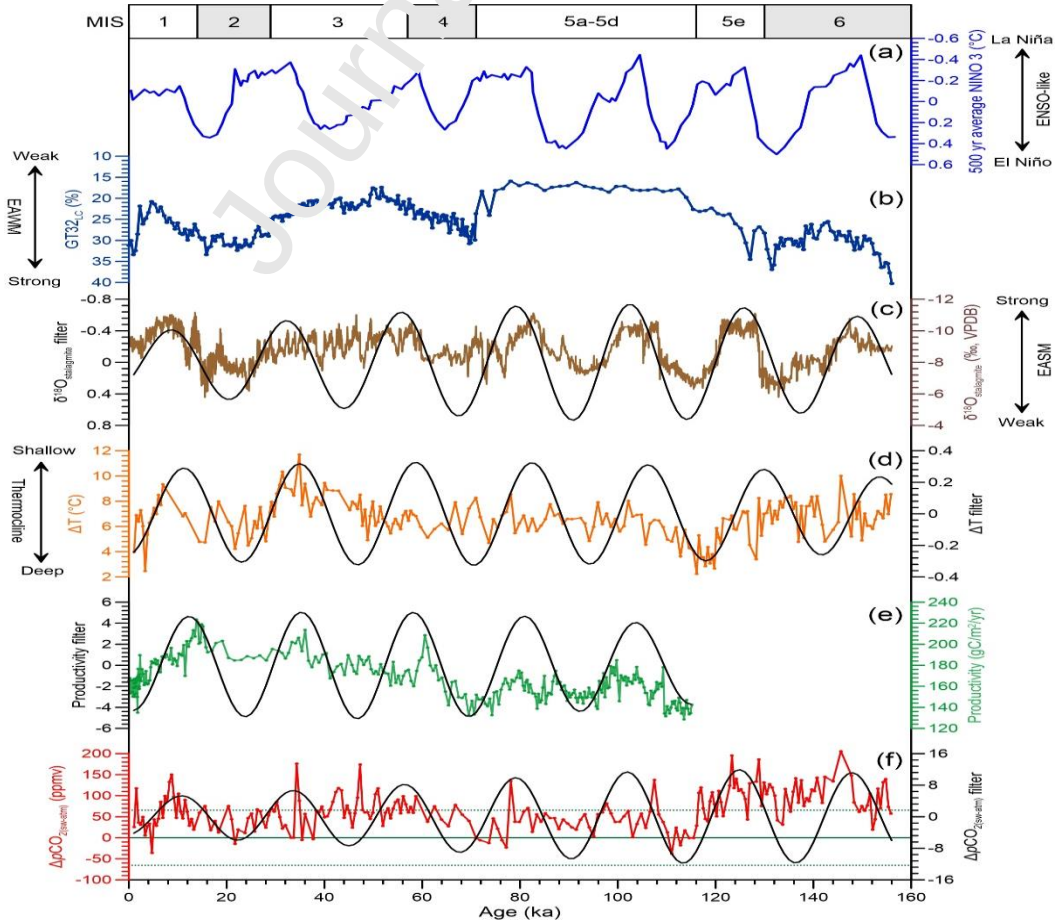

Fig. 3

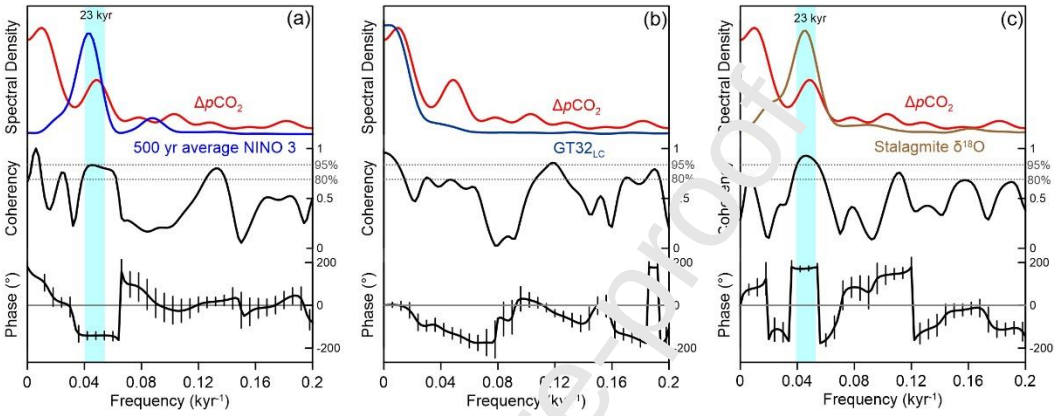

Fig. 4

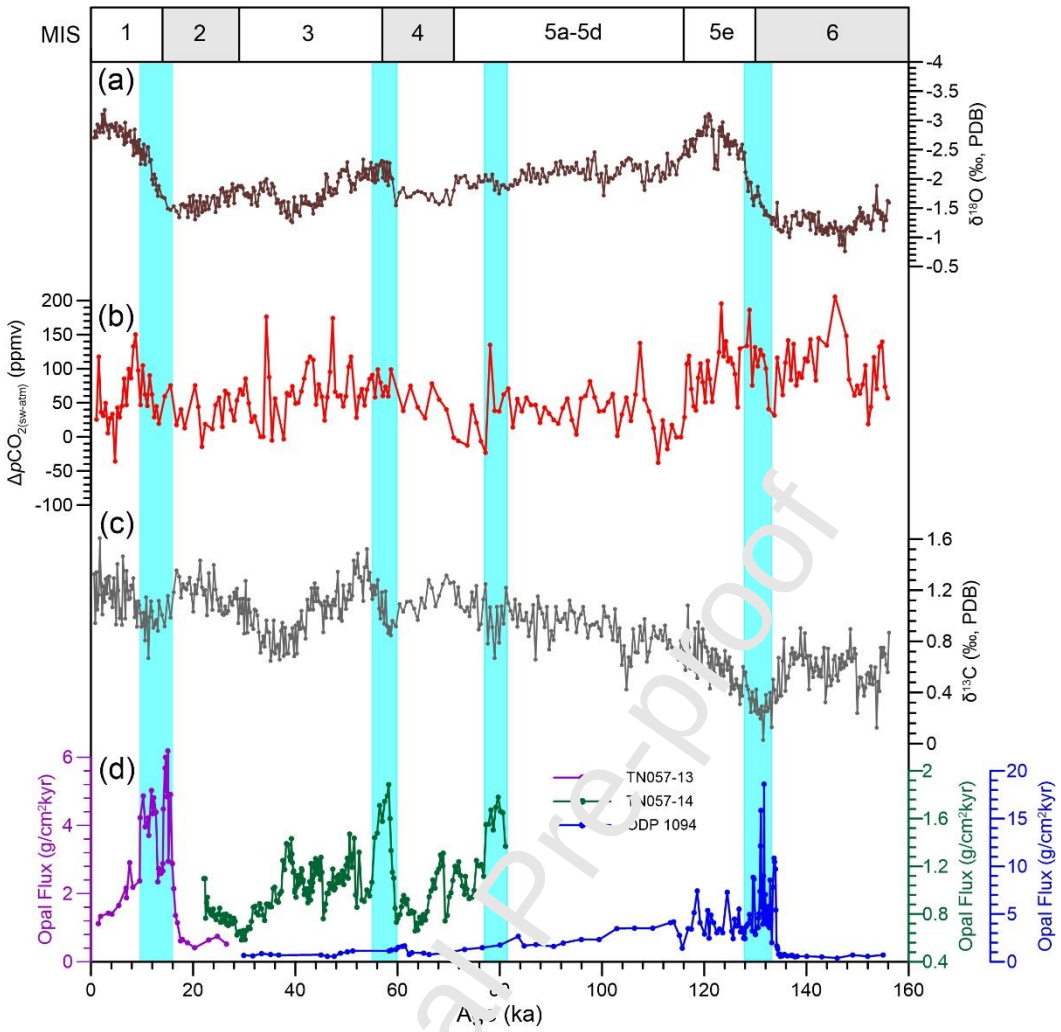

Fig. 5

Declaration of interests

☒ The authors declare that they have no known competing financial interests or personal relationships that could have appeared to influence the work reported in this paper.

☐ The authors declare the following financial interests/personal relationships which may be considered as potential competing interests:

Highlights

- Reconstruction of sea-surface pH and pCO_2 in Western Tropical Pacific since MIS-6
- EAWM and ENSO-like conditions do not affect $\Delta pCO_{2(sw\text{-}atm)}$ of WTP in precession band
- Precession-driven EASM affects air-sea CO_2 exchange by regulating productivity & DOT
- Surface carbonate system in WTP linked to upwelling of Southern Ocean deep waters
- Upwelling strongest during cold-to-warm stage transitions (MIS 6/5, 5b/5a, 4/3, 2/1)